Contribution from the Department of Chemistry, Faculty of Education, Mie University, 1515 Kamihama, Tsu, Mie 514, Japan, Gifu Pharmaceutical University, 6-1 Mitahora-higashi 5, Gifu 502, Japan, and Nara University of Education, Takabatake-cho, Nara 630, Japan

Proton-Induced Switching of Metal–Metal Interactions in Dinuclear Ruthenium and Osmium Complexes Bridged by 2,2′-Bis(2-pyridyl)bibenzimidazole[1]

Masa-aki Haga,*[,2a] Tomo-aki Ano,[2a] Kenji Kano,[2b] and Shinichi Yamabe[2c]

Received March 7, 1991

New dinuclear complexes $[M(L)_2(bpbimH_2)M(L)_2]^{4+}$ (M = Ru, Os; L = bpy, phen; $bpbimH_2$ = 2,2′-bis(2-pyridyl)bibenzimidazole) act as dibasic acids. Both the absorption spectra and oxidation potentials are strongly dependent on the solution pH, which is responsible for the deprotonation of the N–H group on the coordinated bridging ligand. The pK_a values reflect the metal oxidation states, M(II) and M(III). The pK_a values of the mixed-valence dinuclear complexes are quite close to those of each M(II) and M(III) component, which suggests that the mixed-valence complexes have a localized valence structure. The mixed-valence complexes bridged by the protonated ligand $bpbimH_2$ exhibit the intervalence (IT) band at 7300 cm^{-1} for M = Ru and at 9100 cm^{-1} for M = Os, respectively. When the bridging ligand is deprotonated, this IT band is shifted to lower energy at 5880 cm^{-1} for M = Ru and 7700 cm^{-1} for M = Os and intensified. The degree of metal–metal interaction of the deprotonated dinuclear complexes becomes 4–6 times larger than that of the protonated complexes. This proton-induced change of metal–metal interaction can be rationalized by change of HOMO energy levels on deprotonation or protonation in the bridging ligands. Thus, proton transfer in the $bpbimH_2$ bridging dinuclear complexes can be utilized to serve as a trigger signal for switching the metal–metal interaction.

Introduction

Much attention has been paid to the intramolecular electron-transfer process between metal ions in ligand-bridged di- or oligonuclear complexes with regard to the design of photochemical molecular devices[3,4] or the mimetic model of the photosynthetic system in biology.[5] Recently, the supramolecular assemblies composing of oligonuclear metal complexes with bridging ligands have been proposed to have potential as building blocks for synthesizing molecular level chips such as molecular size "wires" and "rectifiers".[6] As a model system of the molecular wire, the mixed-valence complexes separated by a long conjugated chain have been reported to allow the intramolecular propagation of electrons between a donor and an acceptor site. Furthermore, Launay has recently pointed out the possibility of "molecular switching" by proton transfer.[6b]

Chart I. Ligands Used in the Present Study and Their Abbreviations

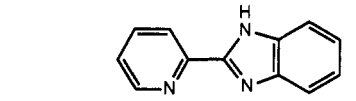

pbimH

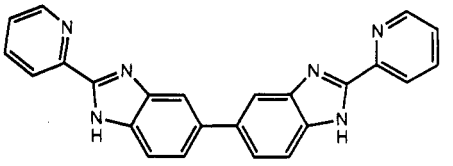

$bpbimH_2$

One of the most important factors is how to design a bridging ligand for synthesizing the functional Ru complexes.[7] Pyridine, pyrazine, and pyrimidine groups have so far been used to bridge the Ru component units for building up the oligonuclear Ru complexes.[3,8] However, these bridging ligands have mainly π-acceptor property.[3,8] On the other hand, the benzimidazole group has a σ/π-donor property[7,9] and furthermore possesses a dissociative N–H proton. Until now, dinuclear complexes with σ/π-donor bridging ligands were relatively sparse.[9a,10,11]

We are interested in tuning the redox and photochemical properties of the dinuclear complexes with σ/π-donor bridging ligands such as benzimidazole groups. Once the benzimidazole unit is coordinated to the metal ion, the imino N–H proton becomes more acidic and can be easily removed. The deprotonation of the bridging ligand may induce a fairly large perturbation on the spectral and redox properties of dinuclear complexes. Here, we report control of the metal–metal interaction by proton transfer

(1) A preliminary paper was presented at the XXVII International Conference on Coordination Chemistry, Broadbeach, Australia, July 2–7, 1989; Abstract W55.
(2) (a) Mie University. (b) Gifu Pharmaceutical University. (c) Nara University of Education.
(3) (a) Ohno, T. *Prog. React. Kinet.* **1988**, *14*, 219–248. (b) Scandola, F.; Bignozzi, C. A.; Chiorboli, C.; Indelli, M. T.; Rampi, M. A. *Coord. Chem. Rev.* **1990**, *97*, 299–312. (c) Petersen, J. D. In *Supramolecular Photochemistry*; Balzani, V., Ed.; Reidel: Dordrecht, The Netherlands, 1987; p 135. (d) Lehn, J.-M. Ibid., p 29. (e) Bignozzi, C. A.; Roffia, S.; Chiorboli, C.; Davila, J.; Indelli, M. T.; Scandola, F. *Inorg. Chem.* **1989**, *28*, 4350–4358. (f) Rillema, D. P.; Callahan, R. W.; Mack, K. B. *Inorg. Chem.* **1982**, *21*, 2589–2596. (g) Ernst, S.; Kaim, W. *Inorg. Chem.* **1989**, *28*, 1520–1528. (h) De Cola, L.; Belser, Ebmeyer, F.; Barigelletti, F.; Vogtle, F.; von Zelewsky, A.; Balzani, V. *Inorg. Chem.* **1990**, *29*, 495–499. (i) Hage, R.; Dijkhuis, A. H. J.; Haasnoot, J. G.; Prins, R.; Reedijk, J.; Buchana, B. E.; Vos, J. G. *Inorg. Chem.* **1988**, *27*, 2185–2189. (j) Shaw, J. R.; Webb, R. T.; Schmehl, R. H. *J. Am. Chem. Soc.* **1990**, *112*, 1117–1123. (k) Schanze, K. S.; Neyhart, G. A.; Meyer, T. J. *J. Phys. Chem.* **1986**, *90*, 2182–2193. (l) Curtis, J. C.; Bernstein, J. S.; Meyer, T. J. *Inorg. Chem.* **1985**, *24*, 385–397. (m) Meyer, T. J. *Prog. Inorg. Chem.* **1983**, *30*, 389–440. (n) Balzani, V.; Scandola, F. In *Photoinduced Electron Transfer. Part D*; Fox, M. A., Chanon, M., Eds.; Elsevier: New York, 1988; p 148. (o) Murphy, W. R.; Brewer, K. J.; Gettliffe, G.; Petersen, J. D. *Inorg. Chem.* **1988**, *28*, 81–84. (p) Rillema, D. P.; Sahai, R.; Matthews, P.; Edwards, A. K.; Shaver, R. J.; Morgan, L. *Inorg. Chem.* **1990**, *29*, 167–175. (q) Denti, G.; Campagna, S.; Sabatino, L.; Serroni, S.; Ciano, M.; Balzani, V. *Inorg. Chem.* **1990**, *29*, 4750–4758.
(4) Balzani, V.; Moggi, L.; Scandola, F. In *Supramolecular Photochemistry*; Balzani, V., Ed.; Reidel: Dordrecht, The Netherlands, 1987; p 1.
(5) Meyer, T. J. *Acc. Chem. Res.* **1989**, *22*, 163–170.
(6) (a) Woitellier, S.; Launay, J. P.; Spangler, C. W. *Inorg. Chem.* **1989**, *28*, 758–762. (b) Launay, J. P. In *Molecular Electronic Devices II*; Carter, F. L., Ed.; Marcel Dekker: New York, 1987; p 39. (c) Hopfield, J. J.; Onuchic, J. N.; Beratan, D. N. *Science* **1988**, *241*, 817–820. (d) Kim, Y.; Lieber, C. M. *Inorg. Chem.* **1989**, *28*, 3990.
(7) Constable, E. C.; Steel, P. J. *Coord. Chem. Rev.* **1989**, *93*, 205.
(8) (a) Ross, H. B.; Boldaji, M.; Rillema, D. P.; Blanton, C. B.; White, R. P. *Inorg. Chem.* **1989**, *28*, 1013–1021. (b) Murphy, W. R.; Brewer, K. J.; Gettliffe, G.; Petersen, J. D. *Inorg. Chem.* **1989**, *28*, 81–84. (c) Toma, H. E.; Auburn, P. R.; Dodsworth, E. S.; Golovin, M. N.; Lever, A. B. P. *Inorg. Chem.* **1987**, *26*, 4257–4263.
(9) (a) Haga, M.; Matsumura-Inoue, T.; Yamabe, S. *Inorg. Chem.* **1987**, *26*, 4148–4154. (b) Rillema, D. P.; Sahai, R.; Matthews, P.; Edwards, A. K.; Shaver, R. J.; Morgan, L. *Inorg. Chem.* **1990**, *29*, 167–175. (c) Haga, M.; Bond, A. M. *Inorg. Chem.* **1991**, *30*, 475–480.
(10) Kaim, W.; Kasack, V. *Inorg. Chem.* **1990**, *29*, 4696–4699.
(11) (a) Krentzien, H.; Taube, H. *J. Am. Chem. Soc.* **1976**, *98*, 6379–6380. (b) Krentzien, H.; Taube, H. *Inorg. Chem.* **1982**, *21*, 4001–4007. (c) Neyhart, G. A.; Meyer, T. J. *Inorg. Chem.* **1986**, *25*, 4807–4808. (d) Hage, R.; Dijkhuis, A. H. J.; Haasnoot, J. G.; Prins, R.; Reedijk, J.; Buchanan, B. E.; Vos, J. G. *Inorg. Chem.* **1988**, *27*, 2185–2189.

0020-1669/91/1330-3843$02.50/0

Table I. pK_a Values and Electrode Potentials for Dinuclear $[M(L)_2(bpbimH_2)M(L)_2]^{4+}$ Complexes in CH_3CN/Buffer (1:1 v/v) at 20 °C[a]

complex	pK_{11}	pK_{12}	pK_{21}	pK_{22}	pK_{31}	pK_{32}	$E°_1$	$E°_2$	$E°_3$	$E°_4$	$E°_5$	$E°_6$
$[Ru(bpy)_2(bpbimH_2)Ru(bpy)_2]^{4+}$	5.8 (5.61)	8.1 (7.12)	1.4	6.9	1.0	2.0	0.94	0.98	0.72	0.97	0.65	0.73
$[Ru(phen)_2(bpbimH_2)Ru(phen)_2]^{4+}$	5.9 (5.51)	7.7 (6.85)	1.5	6.6	1.0	1.9	0.95	1.00	0.68	0.97	0.62	0.70[f]
$[Os(bpy)_2(bpbimH_2)Os(bpy)_2]^{4+}$	5.3 (5.53)	6.9 (7.09)	2.1	5.9	1.9 (1.51)	2.3 (2.46)	0.53	0.58	0.36	0.57	0.31	0.38

[a] The pK_a values in parentheses are obtained spectrophotometrically. The notations for pK_a values and electrode potentials in this table are defined in Scheme I. $E°$ values are in V vs Ag/AgCl.

on the bridging ligand, which can be regarded as a model system for molecular switching. Recently, several reports have appeared regarding the change in electronic interaction by proton transfer.[11] For example, dinuclear ruthenium pentaammine complexes with malononitrile have been observed to increase metal–metal interaction by the deprotonation of bridging malononitrile.[11a] Similarly, the deprotonation of bridged 3,5-bis(pyridin-2-yl)-1,2,4-triazole has been suggested to intensify the metal–metal interaction.[11d] However, none of the complexes were studied for both protonated and deprotonated forms in detail. In the present study, a new dinucleating ligand, 2,2′-bis(2-pyridyl)bibenzimidazole ($bpbimH_2$), in Chart I is introduced. This ligand has a dimeric structure of 2-(2-pyridyl)benzimidazole (pbimH), and the benzimidazole component can act as a feasible moiety for proton equilibria. We focus our attention on the switching property for the metal–metal interaction by proton transfer.

Results and Discussion

Preparations and Characterizations. The novel dinucleating ligand $bpbimH_2$ was prepared by the condensation reaction of 3,3′-diaminobenzidine with picolinic acid in polyphosphoric acid.[12] The stoichiometric reaction between $M(L)_2Cl_2$ (L = bpy, phen; M = Os, Ru) and $bpbimH_2$ (2:1 molar ratio) proceeds smoothly in a boiling ethanol/water mixture. The dinuclear complex $[M(L)_2(bpbimH_2)M(L)_2](ClO_4)_4$ has been isolated as a perchlorate salt. Dinuclear complexes were purified by elution with Sephadex LH-20 column chromatography in methanol/acetonitrile or SP Sephadex C-25 in acetonitrile/buffer. The dideprotonated dinuclear complexes were easily prepared by the reaction of sodium methoxide with protonated complexes $[M(L)_2(bpbimH_2)M(L)_2](ClO_4)_4$ in methanol.

Proton-Transfer Equilibria of the Dinuclear Complexes from Spectrophotometric Studies. The absorption spectra of the dinuclear complexes in CH_3CN/buffer mixture are strongly dependent on the solution pH.

$[Ru(bpy)_2(bpbimH_2)Ru(bpy)_2](ClO_4)_4$ in CH_3CN/buffer (1:1 v/v) exhibits a metal-to-ligand charge-transfer (MLCT) band at 459 nm. The pH dependence of the absorption spectra is shown in Figure 1. From pH 4.34 to 6.48, the MLCT band at 459 nm decreases and a new shoulder appears around 500 nm. Two well-defined isosbestic points at 438 and 477 nm can be seen. A further increase of pH from 6.48 to 9.48 leads to a further decrease of the 459-nm band and finally to the splitting of this band into two clear peaks at 438 and 485 nm, keeping the isosbestic points at 435 and 479 nm. From these spectral changes, sequential acid–base equilibria are present as shown in eq 1, where the

$$[Ru(II)\text{–}bpbimH_2\text{–}Ru(II)]^{4+} \underset{K_{11}}{\rightleftharpoons} [Ru(II)\text{–}bpbimH\text{–}Ru(II)]^{3+} \underset{K_{12}}{\rightleftharpoons} [Ru(II)\text{–}bpbim\text{–}Ru(II)]^{2+} \quad (1)$$

dinuclear complex is abbreviated as $[Ru(II)\text{–}bpbimH_2\text{–}Ru(II)]^{m+}$ and bpbimH and bpbim are used as abbreviations for the mono- and dideprotonated forms of $bpbimH_2$, respectively. The calculated values of pK_{11} and pK_{12} are 5.61 and 7.12 at 20 °C. Similarly, all of the other dinuclear complexes studied here show two stepwise spectral changes throughout the pH range 0–12, which are distinct from those for mononuclear ones. The calculated pK_a values are collected in parentheses in Table I.

The complex in the Os(III)–Os(III) oxidation state generated by the NO^+ oxidation also shows two stepwise acid–base equilibria, while the pK_a values are much lower than those of Os(II)–Os(II) state. This large pK_a shift accompanied by the oxidation state change from Os(II) to Os(III) is attributed to the larger electron-withdrawing property of the higher oxidation state, Os(III).[13]

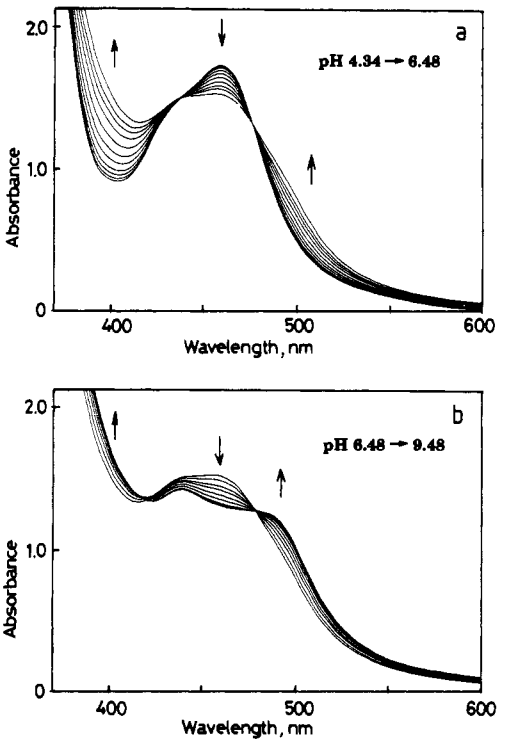

Figure 1. Absorption spectra of $[Ru(bpy)_2(bpbimH_2)Ru(bpy)_2](ClO_4)_4$ (6.6×10^{-5} mol dm^{-3}) at 20 °C in CH_3CN/buffer (1:1 v/v) at various pH values: (a) lower pH region, pH 4.34–6.48; (b) higher pH region, pH 6.48–9.48.

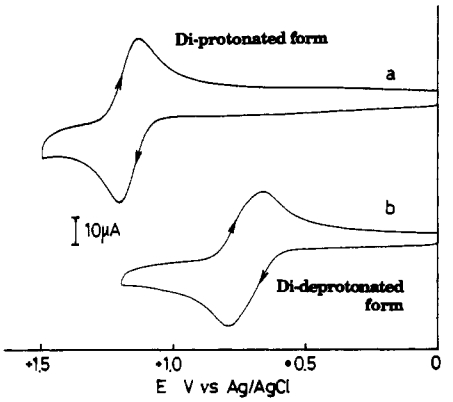

Figure 2. Cyclic voltammograms for $[Ru(bpy)_2(bpbimH_2)Ru(bpy)_2](ClO_4)_4$ (a) and $[Ru(bpy)_2(bpbim)Ru(bpy)_2](ClO_4)_2$ (b) in CH_3CN (0.1 mol dm^{-3} $(TBA)BF_4$) at a glassy-carbon electrode with scan rate = 100 $mV \cdot s^{-1}$. In the same solvent system, the $E_{1/2}$ value for the ferrocenium/ferrocene couple is +0.380 V vs Ag/AgCl.

(12) Three possible geometrical isomers in the free $bpbimH_2$ ligand are anticipated, assuming free rotation between the biphenyl C–C bond. From ^1H NMR (400 MHz) and ^{13}C NMR spectra, only one group of signals for the ring protons and carbons can be observed, which suggests a C_{2v}-type structure.

(13) (a) Bond, A. M.; Haga, M. *Inorg. Chem.* **1986**, *25*, 4507–4514. (b) Hoq, M. F.; Shepherd, R. E. *Inorg. Chem.* **1984**, *23*, 1851–1858.

Scheme I

$$\begin{array}{ccccc}
[\text{Ru(II)–bpbimH}_2\text{–Ru(II)}]^{4+} & \rightleftharpoons & [\text{Ru(II)–bpbimH–Ru(II)}]^{3+} & \rightleftharpoons & [\text{Ru(II)–bpbim–Ru(II)}]^{2+} \\
\mathbf{1} & K_{11} & \mathbf{2} & K_{12} & \mathbf{3} \\
E^\circ_1 \updownarrow e^- & & E^\circ_3 \updownarrow e^- & & E^\circ_5 \updownarrow e^- \\
[\text{Ru(II)–bpbimH}_2\text{–Ru(III)}]^{5+} & \rightleftharpoons & [\text{Ru(II)–bpbimH–Ru(III)}]^{4+} & \rightleftharpoons & [\text{Ru(II)–bpbim–Ru(III)}]^{3+} \\
\mathbf{4} & K_{21} & \mathbf{5} & K_{22} & \mathbf{6} \\
E^\circ_2 \updownarrow e^- & & E^\circ_4 \updownarrow e^- & & E^\circ_6 \updownarrow e^- \\
[\text{Ru(III)–bpbimH}_2\text{–Ru(III)}]^{6+} & \rightleftharpoons & [\text{Ru(III)–bpbimH–Ru(III)}]^{5+} & \rightleftharpoons & [\text{Ru(III)–bpbim–Ru(III)}]^{4+} \\
\mathbf{7} & K_{31} & \mathbf{8} & K_{32} & \mathbf{9}
\end{array}$$

Oxidative Electrochemistry of Dinuclear Complexes. Figure 2 shows the cyclic voltammograms of isolated dinuclear complexes $[Ru(bpy)_2(bpbimH_2)Ru(bpy)_2](ClO_4)_4$ (a) and $[Ru(bpy)_2(bpbim)Ru(bpy)_2](ClO_4)_2$ (b) in CH_3CN. Both complexes show only one oxidation wave.

However, the peak separation, ΔE_p ($=E_{pa} - E_{pc}$), of complex b is larger and the oxidation potential is shifted to the negative direction compared with those of complex a. A two-electron oxidation process is confirmed by the controlled-potential electrolysis of complex a at +1.3 V vs Ag/AgCl in CH_3CN. The potential $E_{1/2}$–pH diagram for $[Ru(bpy)_2(bpbimH_2)Ru(bpy)_2](ClO_4)_4$ in CH_3CN/buffer (1:1 v/v) was analyzed according to the procedure in the Experimental Section. The following pK_a values are obtained: $pK_{11} = 5.8$, $pK_{12} = 8.1$, $pK_{31} = 1.0$, and $pK_{32} = 2.0$ (see Scheme I and Table I).

The peak separation, ΔE_p, of cyclic voltammograms for dinuclear $[Ru(bpy)_2(bpbimH_2)Ru(bpy)_2](ClO_4)_4$ was obviously larger than the theoretical one (28.5 mV at 25 °C) predicted from a one-step two-electron mechanism. However, the peak separation was practically independent of scan rate v at $v < 50$ mV·s^{-1}. The observed peak separations ranged from 50 to 120 mV, depending on pH. This behavior can be interpreted in terms of two-step one-electron charge-transfer reactions such as

$$[\text{Ru(II)–Ru(II)}] \underset{e^-}{\overset{E_{1/2}^1}{\rightleftharpoons}} [\text{Ru(II)–Ru(III)}] \underset{e^-}{\overset{E_{1/2}^2}{\rightleftharpoons}} [\text{Ru(III)–Ru(III)}] \quad (2)$$

and the standard potential in each step, $E_{1/2}^1$ or $E_{1/2}^2$, can be determined by using the working curves for the relation between the potential separation ΔE_p and ΔE ($=E_{1/2}^2 - E_{1/2}^1$) derived by Richardson and Taube.[14] By application of this operation to the present Ru dinuclear system, the presence of the mixed-valence Ru(II)–Ru(III) state can be recognized. The pH dependence of the evaluated $E_{1/2}^1$ and $E_{1/2}^2$ values is shown in Figure 3. The $E_{1/2}^1$–pH profile consists of five lines. At low pH 0–1.4, the slope becomes 0 mV/pH, indicative of a one-electron process with no proton transfer. Over the pH range 1.2–5.8, the slope of the plot of $E_{1/2}^1$ vs pH is −60 mV/pH, which is consistent with a one-proton, one-electron reaction. At $5.8 < pH < 6.9$, $E_{1/2}^1$ is again independent of pH. Over the pH range 6.9–8.1, a plot of $E_{1/2}^1$ vs pH is linear with a slope of −60 mV/pH, consistent with a one-proton, one-electron process. Above pH > 8.1, the potentials are again pH independent. Spectrophotometric data and $E_{1/2}$ vs pH plots for $[Ru^{II}(bpy)_2(bpbimH_2)Ru^{II}(bpy)_2]^{4+}$ indicate that *three* species exist throughout the pH range studied. The $E_{1/2}^1$–pH profile indicates that three species also exist for mixed-valent $[Ru^{II}(bpy)_2(bpbimH_2)Ru^{III}(bpy)_2]^{5+}$.

The intercept of the two straight lines gives pK_a values. Therefore, two break points, 5.8 and 8.1, correspond to the pK_a values for the Ru(II)–Ru(II) state and the other two points, 1.4 and 6.9, correspond to those for the mixed-valence Ru(II)–Ru(III) state. These pK_a values can be proved by applying the nonlinear regression analysis to the $E_{1/2}^1$ vs pH profile (see eq 3 in the Experimental Section). Similar discussion holds for the $E_{1/2}^2$ vs pH profile. The break points of 1.0 and 2.0 for the $E_{1/2}^2$ vs pH profile correspond to the pK_a values for the Ru(III)–Ru(III) state. Consequently, including eqs 1 and 2, we can summarize the acid–base and redox equilibria of $[Ru(bpy)_2(bpbimH_2)Ru(bpy)_2]^{4+}$ in Scheme I. In the scheme, bold numbers are those defined in Figure 3 and the bpy ligands are omitted. According to the notation in Scheme I, the calculated values of pK_a and the standard potentials, E°, are given in Table I.

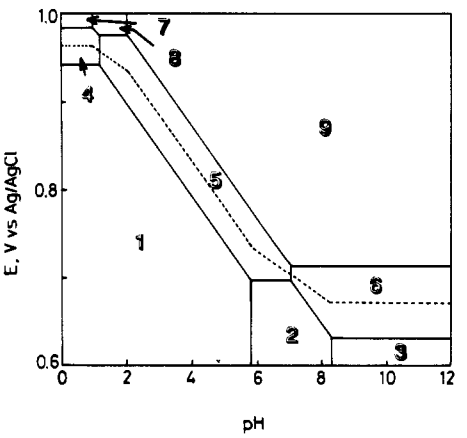

Figure 3. Oxidation potentials, $E_{1/2}^1$ and $E_{1/2}^2$, vs pH diagrams for $[Ru(bpy)_2(bpbimH_2)Ru(bpy)_2](ClO_4)_4$ in CH_3CN/buffer (1:1 v/v) at 20 °C. The broken line indicates the plot of $E_{1/2}$ ($=E_{1/2}^1 + E_{1/2}^2$) vs pH, which is in agreement with the borderline with filled circles of the diagram in Figure 7. Key: $[Ru(II)\text{–bpbimH}_2\text{–Ru(II)}]^{4+}$ (**1**); $[Ru(II)\text{–bpbimH–Ru(II)}]^{3+}$ (**2**); $[Ru(II)\text{–bpbim–Ru(II)}]^{2+}$ (**3**); $[Ru(II)\text{–bpbimH}_2\text{–Ru(III)}]^{5+}$ (**4**); $[Ru(II)\text{–bpbimH–Ru(III)}]^{4+}$ (**5**); $[Ru(II)\text{–bpbim–Ru(III)}]^{3+}$ (**6**); $[Ru(III)\text{–bpbimH}_2\text{–Ru(III)}]^{6+}$ (**7**); $[Ru(III)\text{–bpbimH–Ru(III)}]^{5+}$ (**8**); $[Ru(III)\text{–bpbim–Ru(III)}]^{4+}$ (**9**).

The pK_a values for the Ru(II)–Ru(II) state obtained electrochemically (5.8 and 8.1) agree reasonably with the spectrophotometrically determined values (5.61 and 7.12) in eq 1. The pK_a values for the Ru(III)–Ru(III) state are 5–6 pH units smaller than those for the Ru(II)–Ru(II) state. The difference between the first and second pK_a values, ΔpK_a ($=pK_{x2} - pK_{x1}$; $x = 1$ and 3), is about 2 pH units for the Ru(II)–Ru(II) state and 1 pH unit for the Ru(III)–Ru(III) state. On the other hand, the pK_a values for the mixed-valence Ru(II)–Ru(III) state are 1.4 and 6.9, and the difference between the two, ΔpK_a, is about 6 pH units. This large pK_a difference for the mixed-valence Ru complexes suggests that the electron may not be delocalized.

All of the other dinuclear complexes show analogous pH dependence of $E_{1/2}$. The pK_a data and the standard potentials at pH = 0 are also collected in Table I. The following relation is recognized: $pK_{31} < pK_{21} < pK_{32} \ll pK_{11} < pK_{22} < pK_{12}$.

Factors Affecting the pK_a or the Oxidation Potential. Effect of the Metal and Its Oxidation State. The pK_a difference between the homovalence M(II)–M(II) and M(III)–M(III) complexes is about 4–6 pH units for the pK_{x1} or pK_{x2} value, while the difference between pK_{x1} and pK_{x2} within each homovalence complex is about 1–2 pH units. On the other hand, the pK_a value for the mixed-valence M(II)–M(III) complexes is considered to reflect the amount of the valence delocalization. If the valence is trapped such as M(II)–M(III), the pK_a value of each mononuclear unit,

(14) Richardson, D. E.; Taube, H. *Inorg. Chem.* **1981**, *20*, 1278–1285.

Table II. Near-Infrared Spectral Data for Mononuclear $[Ru(bpy)_2(bpbimH_2)]^{m+}$ and Dinuclear $[M(bpy)_2(bpbimH_n)M'(bpy)_2]^{m+}$ Complexes in CH_3CN[a]

M-M'	n	m	ν_{max}, cm^{-1} (ϵ, M^{-1} cm^{-1})		
			IT transition	LMCT (L(bpbimH$_2$) π–dπ)	dπ–dπ transition
Ru(III)		3		13900 (2900), 9800 sh	
Ru(II)-Ru(III)	2[b]	5	7300 (<100)	14300 (2700), 9800 sh	
Ru(III)-Ru(III)	2[b]	6		14400 (5600), 10500 sh	
Ru(II)-Ru(III)	0	3	5880 (2000)	12300 (4200)	
Ru(III)-Ru(III)	0	4		12400 (8600), 8600 (5200)	
Os(II)-Os(III)	2[b]	5	9100 (<20)	18100 (2000), 14500 sh	5380 (460), 4380 (1000)
Os(III)-Os(III)	2[b]	6		18200 (3800), 14500 sh	5380 (930), 4380 (2100)
Os(II)-Os(III)	0	3	7700 (420)	15000 (2800), 11000 sh	6170 (300), 4420 (1100)
Os(III)-Os(III)	0	4		15000 (5500), 11000 sh	6170 (600), 4420 (2300)

[a] These data are derived from Figures 4 and 5. The extinction coefficients of the IT transition have been corrected by the comproportionation constant, K_{com}. [b] Measured in the presence of 0.1 mM $HClO_4$.

M(II) and M(III), would remain almost unchanged. When the valence is delocalized such as M(2.5)–M(2.5), the pK_a value moves to a new M(II)–M(III) intermediate pK_a. In the present system, the larger difference between pK_{x1} and pK_{x2} is observed, and further each pK_a value is close to that for the component M(II) and M(III) complex. This result indicates the electron is *localized* in the mixed-valence complexes.

Effect of Deprotonation. The oxidation potential is shifted to the negative direction (~0.3 V) upon deprotonation. The potential difference between the first and the second process, ΔE ($=E^\circ_2 - E^\circ_1$), is related to the comproportionation constant K_{com}. This gives a measure of the stability for the mixed-valence complexes.

$$M(II)\text{-}M(II) + M(III)\text{-}M(III) \overset{K_{com}}{\rightleftharpoons} 2M(II)\text{-}M(III)$$

The protonated dinuclear complexes have the potential difference ΔE of 40–50 mV. When they are deprotonated, the ΔE values become about twice larger (~80 mV). This result suggests that the deprotonation relatively stabilizes the mixed-valence complexes. The K_{com} value for the present system ranges from 5 to 23, which is comparable to that of $[Ru(bpy)_2Cl(4,4'\text{-bpy})Ru(bpy)_2Cl]^{4+}$.[15]

The stability of the mixed-valence complexes may be affected by several factors such as the electrostatic and magnetic superexchange interactions and electron delocalization.[16] The total charge of the complex decreases from +4 to +2 by the deprotonation, and thus the electrostatic repulsion between metal ions decreases. In addition, electrostatic attraction between cationic metal and anionic bridging ligand may arise. Thus, the Coulombic contribution for the stability of the mixed-valence complexes is relatively large. Recently, anionic bridging ligands such as thiocyanate, selenocyanate, and bibenzimidazolate have been reported to stabilize mixed-valence complexes.[9a,16d] Furthermore, the ligand π–M(III) dπ orbital interaction affects the stability of the mixed-valence complexes, when the bridging ligand has a σ/π-donor property such as 2,2'-bibenzimidazolate.[9a] In the present bpbimH$_2$ mixed-valence system, the L π–dπ M(III) interaction is similarly present and intensified by the deprotonation as discussed below.

Intervalence Charge-Transfer (IT) Bands in the Mixed-Valence Complexes. While the original complexes are transparent in the near-infrared region (>750 nm), their oxidative spectroelectrochemistry exhibits rich near-infrared spectra. Figure 4a shows the near-infrared absorption spectra of $[Ru(bpy)_2(bpbimH_2)Ru(bpy)_2]^{m+}$ in CH_3CN. The Ru(III)–Ru(III) complex (m = 6) shows a broad band at 14400 cm^{-1} with a shoulder around 10500 cm^{-1}. A similar band at 13900 cm^{-1} is also observed in the mononuclear $[Ru(bpy)_2(bpbimH_2)]^{3+}$ complex.[17] These absorption bands can be assigned as a ligand bpbimH$_2$ π-to-metal dπ (LMCT) transition. The mixed-valence Ru(II)–Ru(III)

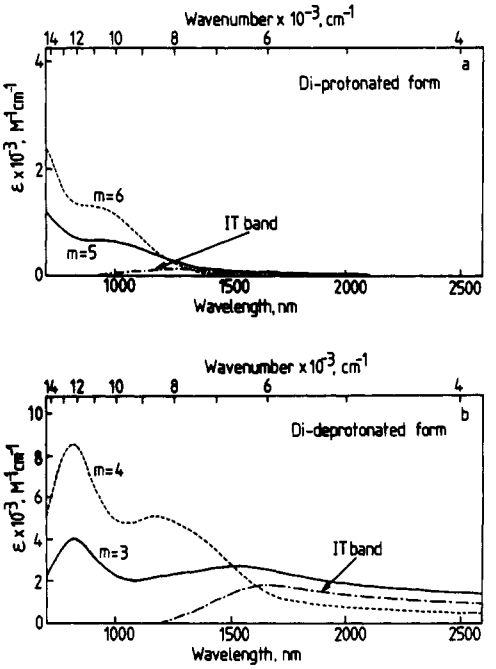

Figure 4. Near-infrared spectra of $[Ru(bpy)_2(bpbimH_2)Ru(bpy)_2]^{m+}$ (a) and $[Ru(bpy)_2(bpbim)Ru(bpy)_2]^{m+}$ (b) in CH_3CN obtained by controlled-oxidative electrolysis. In (a), the intervalence (IT) band is calculated from the direct subtraction of half of the [Ru(III)–Ru(III)] spectrum (m = 6) from the [Ru(II)–Ru(III)] spectrum (m = 5). Similar substraction is made in (b).

complex (m = 5) exhibits a very weak, broad band at 7300 cm^{-1} on the edge of a LMCT band at 14400 cm^{-1}, which can be assigned to an IT transition.[18] This assignment is confirmed by disappearance of this band when the complex was fully oxidized.

In contrast, all the near-infrared bands are intensified and shifted to lower energy in the dideprotonated $[Ru(bpy)_2(bpbim)Ru(bpy)_2]^{m+}$ (m = 3, 4), as shown in Figure 4b. The fully oxidized deprotonated Ru(III)–Ru(III) shows two strong bands at 8600 and 12400 cm^{-1}. These bands can be characterized as LMCT transitions by comparison with the spectra of the protonated dinuclear complex and other complexes reported previously.[19] The red shift of these bands by deprotonation also supports the assignment of the LMCT band, since the deprotonation destabilizes the bpbim^{2-}-occupied orbitals. After the direct subtraction of half of the Ru(III)–Ru(III) spectrum from the Ru(II)–Ru(III) spectrum, the relatively strong IT band in the deprotonated Ru complex can be recognized at 5880 cm^{-1}.[18]

$[Os(bpy)_2(bpbimH_2)Os(bpy)_2]^{6+}$ exhibits two bands at 4380 and 5380 cm^{-1} of dπ–dπ transitions, in addition to the LMCT

(15) Powers, M. J.; Meyer, T. J. *J. Am. Chem. Soc.* **1980**, *102*, 1289.
(16) (a) Richardson, D. E.; Taube, H. *Coord. Chem. Rev.* **1984**, *60*, 107. (b) Creutz, C. *Prog. Inorg. Chem.* **1983**, *30*, 1. (c) Gagne, R. R.; Spiro, C. L.; Smith, T. J.; Hamann, C. A.; Thies, W. R.; Shiemke, A. K. *J. Am. Chem. Soc.* **1981**, *103*, 4073. (d) Palaniappan, V.; Singru, R. M.; Agarwala, U. C. *Inorg. Chem.* **1988**, *27*, 181 and 3568.
(17) Haga, M.; Anou, T.; Kano, K. To be published.
(18) The profile of the LMCT band is assumed to be the same in Ru(III)–Ru(III) and in the mixed-valence form.
(19) (a) Lever, A. B. P. In *Inorganic Electronic Spectroscopy*, 2nd ed.; Elsevier: New York, 1984; Chapter 5. (b) Krogh-Jespersen, K.; Schugar, H. J. *Inorg. Chem.* **1984**, *23*, 4390–4393.

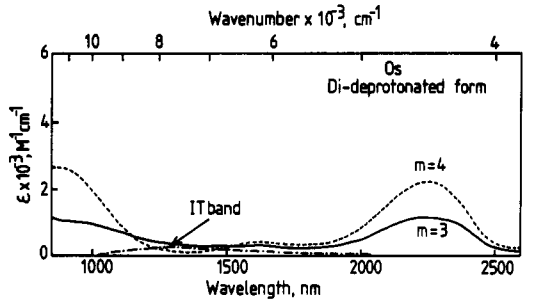

Figure 5. Near-infrared spectra of $[Os(bpy)_2(bpbim)Os(bpy)_2]^{m+}$ in CH_3CN obtained by controlled-oxidative electrolysis. The intervalence band is calculated from the direct subtraction of half of the [Os(III)–Os(III)] spectrum (m = 4) from the [Os(II)–Os(III)] spectrum (m = 3).

Table III. Calculated Parameter H_{AB} for the Degree of Electronic Coupling between the Metal Centers

complex	bandwidth at half-intensity ($\Delta\nu_{1/2}$), cm^{-1}	H_{AB},[a] cm^{-1}
$[Ru(bpy)_2(bpbimH_2)Ru(bpy)_2]^{5+}$	3100	60–80
$[Ru(bpy)_2(bpbim)Ru(bpy)_2]^{3+}$	2520	240–300 (deprotonated)
$[Os(bpy)_2(bpbimH_2)Os(bpy)_2]^{5+}$	3020	30–40
$[Os(bpy)_2(bpbim)Os(bpy)_2]^{3+}$	3040	140–170 (deprotonated)

[a] H_{AB} values depend on the metal–metal distance of the geometrical isomers, which is about 12–15 Å.

bands at 14 500 and 18 200 cm^{-1}. The mixed-valence complex $[Os(bpy)_2(bpbimH_2)Os(bpy)_2]^{5+}$ has a very weak IT band at 9100 cm^{-1} besides $d\pi$–$d\pi$ and LMCT bands. The deprotonation of $[Os(bpy)_2(bpbimH_2)Os(bpy)_2]^{m+}$ (m = 5, 6) results in the lowering of all the transition energies in a manner similar to that in the analogous Ru complexes. Figure 5 shows the near-infrared spectra of $[Os(bpy)_2(bpbim)Os(bpy)_2]^{m+}$ (m = 3, 4). The IT band at 7700 cm^{-1} can be seen. Unfortunately, the reliable near-infrared spectra of mixed-valence monodeprotonated complexes $[M(bpy)_2(bpbimH)M(bpy)_2]^{m+}$ (M = Ru, Os) could not be obtained because of the difficulty of pH adjustment in proton-transfer equilibrium during the oxidative electrolysis. The near-infrared spectral data are summarized in Table II.

The degree of an electronic coupling between the metal centers, H_{AB}, can be evaluated from the position, bandwidth, and intensity of the IT band through the following equation:[20]

$$H_{AB} = 2.05 \times 10^{-2}\left[\frac{\epsilon_{max}\Delta\nu_{1/2}}{\nu_{max}}\right]^{1/2}\left[\frac{\nu_{max}}{r}\right] \text{ (in cm}^{-1}\text{)}$$

where ϵ_{max} is the extinction coefficient (in M^{-1} cm^{-1}), ν_{max} is the wavenumber of the IT absorption maximum (in cm^{-1}), $\Delta\nu_{1/2}$ is the bandwidth at half-intensity (in cm^{-1}), and r is the distance between metal sites (in Å). For the present $bpbimH_2$ bridging system, the value r = 12–15 Å, which depends on the geometrical isomers, was used on the basis of the molecular models. The calculated H_{AB} values are shown in Table III. It can be seen that the H_{AB} values of the deprotonated Ru or Os complexes are 4–6 times larger than those of the protonated Ru or Os complexes.

Effect of Deprotonation of $bpbimH_2$ on the Metal–Metal Interaction. In the previous section, it has been found that the deprotonation magnifies the metal–metal interaction. In order to examine the effect, the electronic structure of our dinucleating ligand, $bpbimH_2$, and its conjugate base is computed with the MNDO method.[21] Figure 6 shows their optimized geometries.

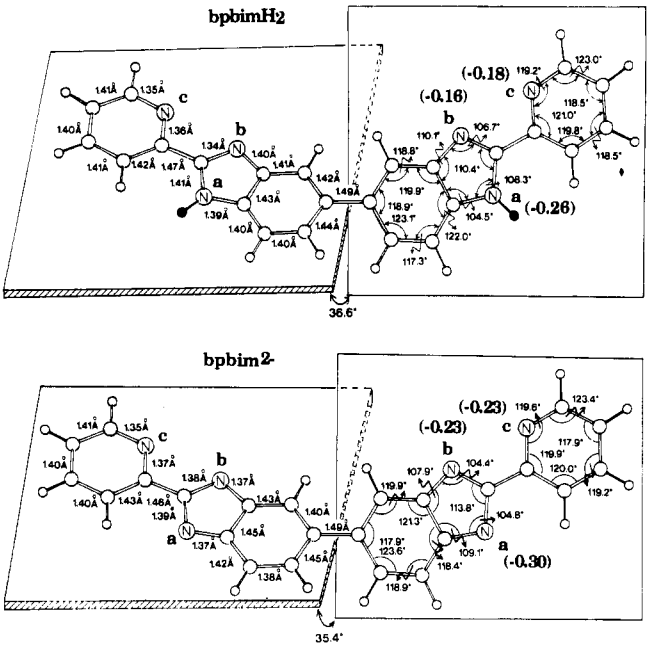

Figure 6. MNDO-optimized geometries of 2,2′-bis(2-pyridyl)bibenzimidazole ($bpbimH_2$) and its dideprotonated molecule. Protons are attached to N_a atoms and are shown by black circles. To distinguish six nitrogen atoms, subscripts a, b, and c are used. In the geometry determination, no assumption such as the planarity of benzene and pyridine rings has been made (i.e., full optimization). Numbers in parentheses stand for anionic net charges on nitrogen atoms a, b, and c.

Scheme II

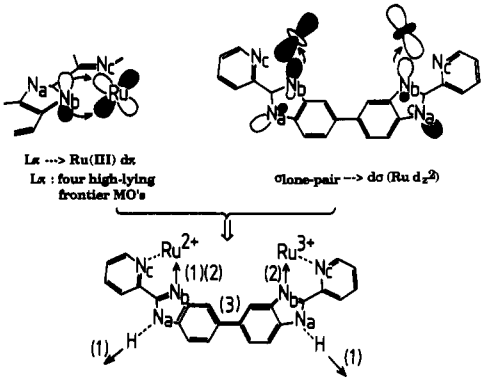

As expected, the biphenyl-type twisting is present, and two molecules are nonplanar. The twisting angle 36.6° of $bpbimH_2$ is close to that 41.6° of biphenyl.[22] However, the pyridine ring is coplanar with the imidazole ring. By the dideprotonation, the geometrical change of the σ skeleton is restricted almost to the imidazole ring and the adjacent benzene ring. A negligible change of the dihedral angle 36.6° → 35.4° and the local geometric change demonstrate that electronic interactions in two coordination sites are independent. This independence seems to be in accord with the large pK_a difference for the mixed-valence Ru complexes ($pK_{21} \ll pK_{22}$) in Table I. Evidently, the anionic nature of nitrogen atoms is strengthened by the dideprotonation as net charges in parentheses of Figure 6 show. This effect leads to the larger metal- - -$bpbim^{2-}$ electrostatic attraction.

More drastic changes are observed in the orbital level. There are four high-lying frontier π MO's in $bpbim^{2-}$, of which orbital energies are −1.7, −2.2, −2.3, and −2.6 eV. In $bpbimH_2$, they are −8.3, −8.6, −8.7, and −9.3 eV. Thus, dideprotonation causes a much larger electron-donating ability. At the same time, in those four MO's, the π frontier densities on the N_b atom ($bpbimH_2$,

(20) (a) Hush, N. S. *Prog. Inorg. Chem.* **1967**, *8*, 391. (b) Creutz, C. *Prog. Inorg. Chem.* **1983**, *30*, 1.

(21) Dewer, M. J. S.; Thiel, W. *J. Am. Chem. Soc.* **1977**, *99*, 4899. The program package AMPAC is used for the MO calculation: AMPAC. QCPE No. 523, Department of Chemistry, Indiana University, Bloomington, IN.

(22) Hellwege, K.-H., Ed. *Landolt-Bornstein Numerical Data and Functional Relationships in Science and Technology. Group II*; Springer-Verlag: Berlin, 1976; Vol. 7, p 387.

Scheme III. Schematic Description of the Molecular Switching Device, Where $[M(bpy)_2]$ (M = Ru or Os) Moieties Are Bridged by $bpbimH_2$ and Proton Transfer Functions as a Trigger Signal

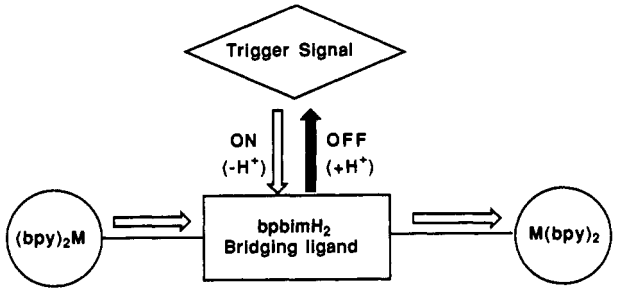

0.24 → $bpbim^{2-}$, 0.41) grow larger than those on the N_c atom ($bpbimH_2$, 0.03 → $bpbim^{2-}$, 0.05). Thus, the L π → dπ Ru(III) charge-transfer (CT) interaction becomes effective almost exclusively on the N_b atom. The dideprotonation also reorganizes σ-lone-pair orbitals. In $bpbimH_2$, all four chelate-type orbitals are nearly of −11-eV energies. In $bpbim^{2-}$, six lone-pair orbitals are classified approximately into three energy groups, −4.5, −5.0, and −5.9 eV. Two −5.9-eV orbitals are of the N_c (in the pyridine ring) lone pair. Therefore, through the high-lying four σ MO's of −4.5 and −5.0 eV, the metal---N_b interaction becomes stronger than the metal---N_c one in $bpbim^{2-}$. In Scheme II, the deprotonation effect (i.e., the localization of interaction) is shown.

(1) The deprotonation enhances the donating power of the π- and σ-electron densities on the N_b atom. (2) The coordinated metal ion approaches the N_b atom owing to the effective L π → dπ and $\sigma_{\text{lone pair}}$ → dσ(d_{z^2} or $d_{x^2-y^2}$) CT's. In the X-ray structure of $[(Ru(bpy)_2)_2(bpt)]^{3+}$, significant shortening of the ruthenium–nitrogen distances has been observed for the nitrogen site with a better σ-donor property.[23] (3) The metal–metal interaction through the deprotonated bridging ligand, $bpbim^{2-}$, is larger than that through the neutral one, $bpbimH_2$, in two respects. One is the shortening of the distance r by the deprotonation. The other is that the enhanced metal coordination effect is transmitted well to the partner metal via the least σ-skelton route without the dispersal of the effect on the terminal pyridine ring. The σ/π-donor ability at the N_b atom is strengthened cooperatively by the deprotonation at N_a, leading to the larger metal–metal interaction. Furthermore, the larger H_{AB} value for the Ru mixed-valence complexes, compared to that for the Os complexes (Table III), can be explained by the closer π-orbital energy levels of bridging ligand to the vacant dπ levels of Ru relative to Os.

As a consequence, the proton transfer on the bridging ligand can alter the metal–metal interaction. Although several Ru dinuclear complexes have been reported to change the metal–metal interaction by the acid–base equilibria, none of the complexes were stable in both protonated and deprotonated forms. The present work has elucidated the correlation thoroughly by the use of stable complexes.

Concluding Remarks

The bridging $bpbimH_2$ ligand enables the dinuclear complex to act as a diprotic acid. The oxidation potential of the dinuclear complex is shifted to the negative direction, accompanied by the deprotonation. Furthermore, the metal–metal interaction becomes stronger when the complex is deprotonated. Since the proton transfer can be regarded as a trigger signal to change the metal–metal interaction or the structure of the complex, these findings can offer the basic idea for the design of molecular level devices such as a molecular switch (see Scheme III).

Experimental Section

Materials. Tetra-*n*-butylammonium tetrafluoroborate ($(TBA)BF_4$) was prepared by standard techniques,[24] recrystallized three times from ethanol/water mixtures and then ethyl acetate/pentane, and vacuum-dried at 70 °C for 12 h. Acetonitrile was dried over phosphorus pentoxide twice and then distilled over CaH_2 under nitrogen. The water used in the measurements was deionized and then distilled in an all-glass apparatus. All other chemicals were of analytical grade and were used as supplied. Buffer systems and the pH ranges employed were as follows: $HClO_4$–$NaClO_4$, pH 0–2; Robinson–Britton buffer, pH 2–11.[25]

Preparation. The starting complexes $Ru(bpy)_2Cl_2\cdot 2H_2O$, $Ru(phen)_2Cl_2$, and $Os(bpy)_2Cl_2$ (bpy = 2,2′-bipyridine; phen = 1,10-phenanthroline) were prepared by the literature methods.[25]

Dinucleating Ligand 2,2′-Bis(2-pyridyl)bibenzimidazole ($bpbimH_2$). *Caution! Extreme care should be exercised in handling 3,3′-diaminobenzidine because of its marked carcinogenic activity.* Both 3,3′-diaminobenzidine (4 g, 18.7 mmol) and 2-picolinic acid (4.7 g, 38.2 mmol) were mixed in polyphosphoric acid (20 cm^3) freshly prepared from phosphorus pentoxide and phosphoric acid, and the mixture was heated at 150 °C for 8 h. After having been cooled to 80 °C, the deep red viscous solution was poured into 500 cm^3 of water with vigorous stirring. The resulting greenish yellow precipitate was filtered. The collected precipitate was neutralized with a solution of Na_2CO_3 (70 g) in hot water (500 cm^3). CO_2 gas was evolved, and at the same time the color of the suspended solution became yellowish white. The precipitate was collected and recrystallized from aqueous methanol twice: yield 2.0 g (49%); mp 230–233 °C. Mass spectrum: m/z = 388 (100), 194 (16.4), assigned to M (molecular peak) and M/2 (100 and 16.4 in parentheses represent the intensities referenced to the base peak in the mass spectrum), where $M = {}^{12}C_{24}H_{16}{}^{14}N_6$. Anal. Calcd for $C_{24}H_{16}N_6\cdot H_2O$: C, 70.92; H, 4.46; N, 20.68. Found: C, 70.34; H, 4.31; N, 20.28.

Dinuclear Complexes. *Caution! Perchlorate salts are potentially explosive. Although no detonation tendencies have been observed, caution is advised and handling of only small quantities is recommended.*

(A) Protonated $bpbimH_2$-Bridged Complexes. $[Ru(bpy)_2(bpbimH_2)Ru(bpy)_2](ClO_4)_4\cdot 4H_2O$. A mixture of $Ru(bpy)_2Cl_2\cdot 2H_2O$ (0.75 g, 1.55 mmol) and bridging ligand $bpbimH_2$ (0.30 g, 0.77 mmol) in ethanol/water (1:1 v/v, 60 cm^3) was refluxed for 9 h, during which time the solution became red orange. The solution was evaporated to dryness, and the residue was dissolved in a minimum amount of water. The sample was loaded on a SP-Sephadex C-25 cation-exchange column (3 × 40 cm) and eluted with CH_3CN/buffer (1:1 v/v). When the solution pH was gradually increased, the first yellow band for the mononuclear band was eluted at pH 5, followed by the second red-orange band at pH 9 for the desired dinuclear complex, which was collected. After evaporation of CH_3CN in the eluate, excess $NaClO_4$ (1 g, 7.1 mmol) was added to the solution. The orange precipitate was filtered out, washed with water, and dried in vacuo. Recrystallization from methanol/water gave the orange crystals, 0.52 g (40% yield). Anal. Calcd for $C_{64}H_{48}N_{14}O_{16}Cl_4Ru_2\cdot 4H_2O$: C, 45.62; H, 3.35; N, 11.64. Found: C, 45.16; H, 3.03; N, 11.49.

$[Os(bpy)_2(bpbimH_2)Os(bpy)_2](ClO_4)_4\cdot 6H_2O$. The complex was prepared by following the same procedures as used for the Ru analogue, except that the starting complex $Os(bpy)_2Cl_2$ and a longer refluxing time were used. Yield: 40%. Anal. Calcd for $C_{64}H_{48}N_{14}O_{16}Cl_4Os_2\cdot 6H_2O$: C, 40.47; H, 3.18; N, 10.32. Found: C, 40.28; H, 2.62; N, 10.21.

$[Ru(phen)_2(bpbimH_2)Ru(phen)_2](ClO_4)_4\cdot 4H_2O$. The procedure was the same as that used for the dinuclear Ru–bpy analogue, substituting $Ru(bpy)_2Cl_2$ for $Ru(phen)_2Cl_2$. Anal. Calcd for $C_{72}H_{48}N_{14}O_{16}Cl_4Ru_2\cdot 4H_2O$: C, 48.55; H, 3.17; N, 11.01. Found: C, 48.27; H, 2.88; N, 10.89.

(B) Dideprotonated bpbim-Bridged Complexes. $[Ru(bpy)_2(bpbim)Ru(bpy)_2](ClO_4)_2\cdot 4H_2O$. A methanol (20 cm^3) solution of $[Ru(bpy)_2(bpbimH_2)Ru(bpy)_2](ClO_4)_4\cdot 4H_2O$ (0.40 g, 0.24 mmol) was added to a sodium methoxide solution made up by the dissolution of sodium metal (0.035 g, 1.5 mmol) in methanol (10 cm^3). The solution immediately changed in color from orange to dark red. After being heated for 30 min, the solution was then cooled to 0–5 °C in a refrigerator. The resulting brown microcrystalline solid was collected by filtration and dried in vacuo. Yield: 54%. Anal. Calcd for $C_{64}H_{46}N_{14}O_8Cl_2Ru_2\cdot 4H_2O$: C, 51.79; H, 3.67; N, 13.21. Found: C, 51.45; H, 3.38; N, 13.06.

$[Os(bpy)_2(bpbim)Os(bpy)_2](ClO_4)_2\cdot 4H_2O$. This complex was prepared in a manner similar to $[Ru(bpy)_2(bpbim)Ru(bpy)_2](ClO_4)_2\cdot 4H_2O$, except that the dinuclear complex $[Os(bpy)_2(bpbimH_2)Os(bpy)_2](ClO_4)_4\cdot 6H_2O$ was used. Yield: 60%. Anal. Calcd for $C_{64}H_{46}N_{14}O_8Cl_2Os_2\cdot 4H_2O$: C, 46.24; H, 3.27; N, 11.79. Found: C, 45.85; H, 3.05; N, 11.60.

Physical Measurements. Electronic spectra were obtained on a Hitachi U-3210 spectrophotometer from 200 to 850 nm and a Hitachi 3400 spectrophotometer from 800 to 2600 nm. The pH measurements were made with a TOA Model HM-20E pH meter standardized with buffers of pH 4.01 and 6.86. A 50% acetonitrile/water mixture was employed because of the solubility limit of the present complexes in pure aqueous

(23) Hage, R.; Haasnoot, J. G.; Nieuwenhuis, H. A.; Reedijk, J.; De Ridder, D. J. A.; Vos, J. G. *J. Am. Chem. Soc.* **1990**, *112*, 9245.
(24) Fry, A. J.; Britton, W. E. In *Laboratory Techniques in Electroanalytical Chemistry*; Kissinger, P. T., Heineman, W. R., Eds.; Marcel Dekker: New York, 1984; p 367.
(25) Britton, H. T. S.; Robinson, R. A. *J. Chem. Soc.* **1931**, *458*, 1456.
(26) Lay, P. A.; Sargeson, A.; Taube, H. *Inorg. Synth.* **1986**, *24*, 291–296.

Scheme IV

$$\begin{array}{ccc} [\text{Ru(III)–bpbimH}_2\text{–Ru(III)}]^{6+} & \overset{2e^-}{\rightleftharpoons} & [\text{Ru(II)–bpbimH}_2\text{–Ru(II)}]^{4+} \\ \Big\| K_{31} & & \Big\| K_{11} \\ [\text{Ru(III)–bpbimH–Ru(III)}]^{5+} & \overset{2e^-}{\rightleftharpoons} & [\text{Ru(II)–bpbimH–Ru(II)}]^{3+} \\ \Big\| K_{32} & & \Big\| K_{12} \\ [\text{Ru(III)–bpbim–Ru(III)}]^{4+} & \overset{2e^-}{\rightleftharpoons} & [\text{Ru(II)–bpbim–Ru(II)}]^{2+} \end{array}$$

solution, particularly at higher pH. The "apparent" pH values of this mixture are referred to as pH unless otherwise stated. Spectrophotometric titrations were performed in acetonitrile/water (1:1 v/v) solution, as described previously.[12] In the case of the Os complexes, the Os(III) oxidation state was generated by the chemical oxidation of Os complexes with $NOBF_4$. A graphical analysis can be used to determine the number of species in solution from spectrophotometric data and the absorbance value of the intermediate species. If the absorbance value of a particular solution, at a specific wavelength, i, is denoted by A_{ij}, a plot of $A_{ij} - A_{if}$ at wavelength i vs the corresponding difference $A_{rj} - A_{rf}$ at another wavelength i' will give a straight line. The absorbance value of the intermediate can be obtained as a breakpoint of the lines.[27]

Electrochemical measurements were made at 20 °C with a Yanagimoto P-1100 polarographic analyzer equipped with a Watanabe WX-4401 x-y recorder. The working electrode was a glassy-carbon electrode and the auxiliary electrode was a platinum plate. The reference electrode was a BAS RE-1 Ag/AgCl electrode. The $E_{1/2}$ value for the ferrocenium/ferrocene couple is +0.190 V vs Ag/AgCl in CH_3CN/buffer at pH 7. The spectroelectrochemistry was performed by using a platinum minigrid (80 mesh) working electrode in the thin-layer cell designed originally by Lexa et al.[28] The cell was located directly in the spectrophotometer, and the absorption change was monitored during the electrolysis.

pK_a Determination from the Oxidation Potential $E_{1/2}$ vs pH Diagram. The cyclic voltammogram of $[Ru(bpy)_2(bpbimH_2)Ru(bpy)_2](ClO_4)_4$ also exhibits only one reversible wave in all the pH region examined here. Since this oxidation wave should be ascribed to an overall two-electron process, the half-wave potential $E_{1/2}$ is estimated as the midpoint potential of the reversible voltammogram. Figure 7 shows the half-wave potential, $E_{1/2}$, vs pH diagram for $[Ru(bpy)_2(bpbimH_2)Ru(bpy)_2](ClO_4)_4$. Below pH 1.0 and above pH 8.1, the Ru(II/III) couple is independent of pH. Over the pH range 1.0–2.0 and 5.8–8.1, the $E_{1/2}$ value decreases linearly with increasing pH with a slope −30 mV/pH unit. At 2.0 < pH < 5.8, the slope of $E_{1/2}$ vs pH plots was −60 mV/pH unit. From this result, both $[Ru^{II}(bpy)_2(bpbimH_2)Ru^{II}(bpy)_2]^{4+}$ and $[Ru^{III}(bpy)_2(bpbimH_2)Ru^{III}(bpy)_2]^{6+}$ possess two sequential acid–base equilibria in the examined pH region as shown in Scheme IV, where the Ru oxidation state is shown in parentheses. Under these acid–base equilibria, $E_{1/2}$ of the Ru(III)–Ru(III)/Ru(II)–Ru(II) couple can be expressed by the following equation:[29]

$$E_{1/2} = E_{1/2}^\circ + \frac{RT}{nF} \ln\left(\frac{\alpha_{red}}{\alpha_{ox}}\right) \qquad (3)$$

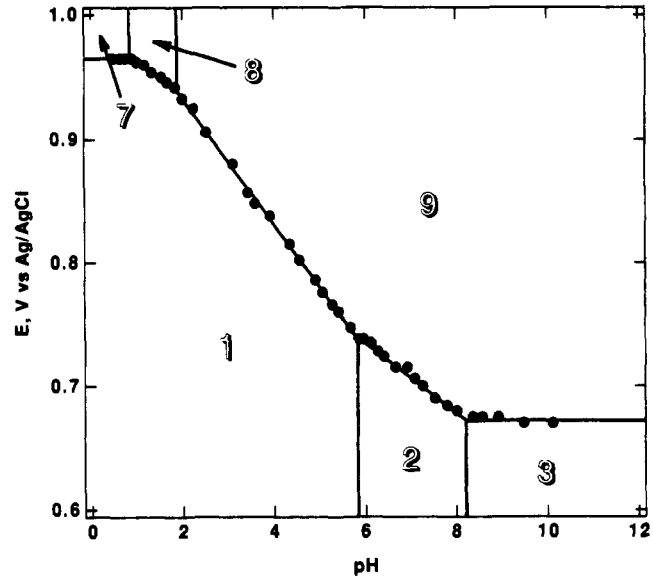

Figure 7. Oxidation potential, $E_{1/2}$, vs pH diagram for $[Ru(bpy)_2(bpbimH_2)](ClO_4)_4$ in CH_3CN/buffer (1:1 v/v) at 20 °C. Key: $[Ru(II)–bpbimH_2–Ru(II)]^{4+}$ (**1**); $[Ru(II)–bpbimH–Ru(II)]^{3+}$ (**2**); $[Ru(II)–bpbim–Ru(II)]^{2+}$ (**3**); $[Ru(III)–bpbimH_2–Ru(III)]^{6+}$ (**7**); $[Ru(III)–bpbimH–Ru(III)]^{5+}$ (**8**); $[Ru(III)–bpbim–Ru(III)]^{4+}$ (**9**).

Here $E_{1/2}^\circ$ is the standard redox potential of the $[Ru(III)–bpbimH_2–Ru(III)]^{6+}/[Ru(II)–bpbimH_2–Ru(II)]^{4+}$ couple, n represents the number of electrons (here $n = 2$), and α_{ox} and α_{red} are given as follows:

$$\alpha_{ox} = 1 + \frac{K_{31}}{[H^+]} + \frac{K_{31}K_{32}}{[H^+]^2} \qquad \alpha_{red} = 1 + \frac{K_{11}}{[H^+]} + \frac{K_{11}K_{12}}{[H^+]^2}$$

According to the equations described above, a nonlinear regression analysis for the $E_{1/2}$ vs pH plots has been performed.

In order to analyze the oxidation potential $E_{1/2}$ vs pH diagram for the two-step one-electron mechanism in Scheme I, a little modification in eq 3 is taken as $n = 1$ and $E_{1/2}^\circ$ = the redox potential for the Ru(II)–$bpbimH_2$–Ru(III)/Ru(II)–$bpbimH_2$–Ru(II) couple.

Acknowledgment. This work was supported by a Grant-in-Aid for Scientific Research (Nos. 01540508 and 02640474) from the Ministry of Education and a grant from the Okasan-Kato Foundation. We thank Prof. Kiyoshi Isobe and Dr. Yoshihito Hayashi at the Institute of Molecular Science for letting us use the near-infrared spectrophotometer and mass spectrophotometer. We also thank Prof. Kunio Shimizu and Dr. Hirotaka Nagao at Sophia University and Prof. Tateo Nomoto at Mie University for their useful discussion.

Registry No. (**1**)$(ClO_4)_4$, 135774-15-1; **2**, 135774-22-0; **3**, 135774-20-8; (**3**)$(ClO_4)_2$, 135774-21-9; **4**, 135774-23-1; **5**, 135774-24-2; **6**, 135774-25-3; **7**, 135774-26-4; **8**, 135774-27-5; **9**, 135774-28-6; $bpbimH_2$, 135774-29-7; $bpbim^{2-}$, 135774-13-9; $Os(bpy)_2Cl_2$, 15702-72-4; $Ru(phen)_2Cl_2$, 85718-09-8; $Ru(bpy)_2Cl_2$, 15746-57-3; $[Os(bpy)_2(bpbimH_2)Os(bpy)_2](ClO_4)_4$, 135774-17-3; $[Ru(phen)_2(bpbimH_2)Ru(phen)_2](ClO_4)_4$, 135774-19-5; $[Os(bpy)_2(bpbim)Os(bpy)_2](ClO_4)_2$, 135799-11-0; 3,3′-diaminobenzidine, 91-95-2; 2-picolinic acid, 98-98-6.

(27) (a) Coleman, J. S.; Varga, L. P.; Mastin, S. H. *Inorg. Chem.* **1970**, *9*, 1013. (b) Long, C.; Vos, J. *Inorg. Chim. Acta* **1984**, *89*, 125. (c) Crutchley, R. J.; Kress, N.; Lever, A. B. P. *J. Am. Chem. Soc.* **1983**, *105*, 1170.
(28) Lexa, D.; Saveant, J. M.; Zickler, J. *J. Am. Chem. Soc.* **1977**, *99*, 2786.
(29) (a) Clark, W. M. In *Oxidation-Reduction Potentials of Organic Systems*; The Williams & Wilkins Co.: Baltimore, MD, 1960; Chapter 4. (b) Meites, L. In *Polarographic Techniques*, 2nd ed.; Interscience: New York, 1965; Chapter 5.